APL Photonics

Invited Article: An active terahertz polarization converter employing vanadium dioxide and a metal wire grating in total internal reflection geometry

Cite as: APL Photonics 3, 051604 (2018); https://doi.org/10.1063/1.5010940
Submitted: 27 October 2017 • Accepted: 04 January 2018 • Published Online: 09 February 2018

Xudong Liu, Xuequan Chen, Edward P. J. Parrott, et al.

Invited Article: An active terahertz polarization converter employing vanadium dioxide and a metal wire grating in total internal reflection geometry

Xudong Liu,[1,a] Xuequan Chen,[1,a] Edward P. J. Parrott,[1] Chunrui Han,[1] Georges Humbert,[2] Aurelian Crunteanu,[2] and Emma Pickwell-MacPherson[1,3,b]

[1]*Department of Electronic Engineering, The Chinese University of Hong Kong, Hong Kong*
[2]*XLIM Research Institute, UMR 7252 CNRS/University of Limoges, Limoges, France*
[3]*Department of Physics and Astronomy, Warwick University, Coventry, United Kingdom*

(Received 27 October 2017; accepted 4 January 2018; published online 9 February 2018)

Active broadband terahertz (THz) polarization manipulation devices are challenging to realize, but also of great demand in broadband terahertz systems. Vanadium dioxide (VO_2) shows a promising phase transition for active control of THz waves and provides broadband polarization characteristics when integrated within grating-type structures. We creatively combine a VO_2-based grating structure with a total internal reflection (TIR) geometry providing a novel interaction mechanism between the electromagnetic waves and the device, to realize a powerful active broadband THz polarization-controlling device. The device is based on a Si-substrate coated with a VO_2 layer and a metal grating structure on top, attached to a prism for generating the TIR condition on the Si-VO_2-grating interface. The grating is connected to electrodes for electrically switching the VO_2 between its insulating and conducting phases. By properly selecting the incident angle of the THz waves, the grating direction, and the incident polarization state, we first achieved a broadband intensity modulator under a fused silica prism with an average modulation depth of 99.75% in the 0.2-1.1 THz region. Additionally, we realized an active ultra-broadband quarter-wave converter under a Si prism that can be switched between a 45° linear rotator and a quarter wave converter in the 0.8-1.5 THz region. This is the first demonstration of an active quarter-wave converter with ultra-broad bandwidth performance. Our work shows a highly flexible and multifunctional polarization-controlling device for broadband THz applications. https://doi.org/10.1063/1.5010940

INTRODUCTION

Terahertz technology has shown versatility as an academic tool to study a wide range of systems, including chemical systems in both solid and liquid forms, medical imaging and spectroscopy, and industrial process control and testing.[1–5] A key element in the growing interest of the terahertz field has been the continued improvement in the development of robust terahertz sources and detectors, such as the air-plasma techniques pioneered over the last decade,[6,7] which have unlocked ever higher powers and broader spectral ranges. However, there is still a lack of active THz polarization-manipulation components, including THz waveplates and polarizers, that are able to work across wide frequency bands. Passive wire-grid polarizers have been demonstrated with extinction ratios (defined as the intensity ratio between the fields transmitted from the blocking direction and passing direction of

[a]X. Liu and X. Chen contributed equally to this work.
[b]Author to whom correspondence should be addressed: e.pickwell.97@cantab.net.

the polarizer in the dB scale) exceeding 60 dB or more across broadband regions, and such devices are now available commercially.[8–14] Closely stacked and rotated thin film wire grid polarizers have been demonstrated by Cong *et al.* to be able to rotate the polarization state of an incoming linearly polarized terahertz beam, demonstrating a 90° rotation for a relatively broad bandwidth of 0.8 THz.[15] Metamaterial-based designs have demonstrated a narrow band phase modulator based upon electrically controlling the strength of a resonance within a split ring system.[16] Asymmetric resonance structures in orthogonal orientations coupled to a wire grating can produce a broadband polarization conversion with an arbitrary phase difference.[17,18] Waveplates are not confined to metallic metamaterials; as the Koch group have shown, it is possible to generate broadband terahertz waveplates using designs based on paper sheets.[19,20] Vanadium dioxide (VO_2) is a promising material for active THz components[21] due to its ability to perform a reversible phase transition between an insulating to a conducting state, transition which can be realized by thermal, electrical, and optical means. Active VO_2 broadband switchable intensity modulators[22,23] and actively controlled VO_2 based gratings and polarizers[24,25] have been already demonstrated. These studies opened a new way of manipulating THz lights by VO_2. However, these devices only focused on the intensity modulation in transmission geometry. More potential applications by employing the switchable characteristics of VO_2 to realize active polarization control were not explored by these studies.

In our previous work, we developed a new theory and technique to manipulate the terahertz signal by controlling the conductivity of the interface in a total internal reflection (TIR) geometry.[26,27] The theory and experimental results in this work show a significantly improved modulation in TIR geometry than in a traditional transmission setup. We extended the theory to anisotropic conductive interfaces, such as metallic gratings on the TIR interface.[28] The work proposed a theory describing the reflection characteristics from a grating surface in TIR conditions. Based on this theory, a single device capable of either rotating an input polarization by 45°, converting the polarization from linear to circular and vice versa, or a half-waveplate polarization conversion was demonstrated. In this paper, we further developed the concept of a passive THz polarization converter to active devices by incorporating a VO_2 thin film with a grating in TIR geometry. In this way, we have now demonstrated an active broadband intensity modulator with an average modulation depth of 99.75% in the 0.2-1.1 THz region and an active quarter wave converter in the 0.8-1.5 THz region. [For clarity, the modulation depth (MD) describes the intensity modulation capabilities and is defined as $MD = (1 - Intensity_{OFF}/Intensity_{ON}) \times 100\%$.]

DEVICE FABRICATION AND SYSTEM ESTABLISHMENT

Figure 1(a) shows the structure of the fabricated device. The 100 nm thick VO_2 film was deposited on a 1 mm thick Si(100) substrate using the electron beam evaporation of a metallic vanadium target under oxygen atmosphere using similar experimental conditions reported previously for VO_2 layer deposition on sapphire substrates.[29] Contrary to the VO_2 growth on c-cut sapphire substrates resulting in (002) mono-oriented films, the X-ray diffraction (XRD) analysis of VO_2 films deposited on Si substrates shows that they are polycrystalline, but all diffraction peaks appearing in the θ-2θ diffraction spectra are consistent with the VO_2's monoclinic M1, insulating phase. Photolithography and electron-beam evaporation are used to pattern the 10 μm gold wire grating on the VO_2 surface

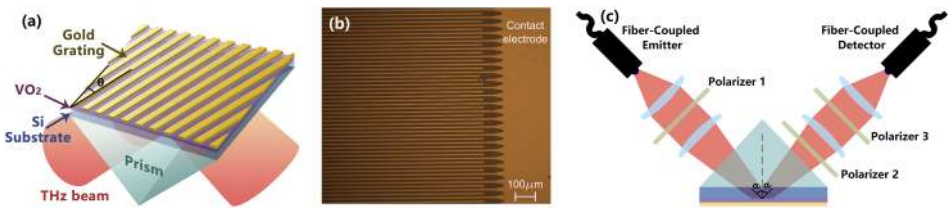

FIG. 1. (a) Schematic diagram of the VO_2 device and its combination with the prism in the measurement system. (b) Microscope image of the grating-VO_2 surface. (c) Schematic diagram of the measurement system and the beam interaction with the device at normal incidence to the prism surface.

with a period of 20 μm. A microscope image of the grating is shown in Fig. 1(b), highlighting that the metal grating structure acts also as electrodes for electrical activation of the VO_2 phase transition. A prism was put under the Si substrate to refract the THz light into the Si plate with a desired incident angle to the Si-VO_2 interface that meets the TIR condition, as shown in Fig. 1(a). The angle between the grating and the *E*-field of *s*-polarized THz light is defined as θ, which can be varied by simply rotating the Si plate.

A fiber-coupled THz-TDS system is established for the measurement, as shown in Fig. 1(c). The system was built based on Tera K15 from Menlo Systems GmbH. The incident angle of the setup can be freely adjusted as to the measurement requirement. The THz beam was manipulated by four TPX lenses and focused onto the Si-VO_2 interface. Three wire-grid polarizers were used in this system, with polarizers 1 and 3 being the thin-film bi-layer polarizers made by Huang *et al.*[10] and polarizer 2 from Microtech Instruments. Polarizer 1 was used to linearly filter the incident light into a desired direction. Polarizer 2 was an analyzer to select the reflected *p*- or *s*-component, while polarizer 3 was 45° rotated to be parallel to the major detection direction of the detector so as to create an equal sensitivity on the detection of the *p*- and *s*-components.

RESULTS AND DISCUSSION

The *s*- and *p*-reflection coefficients of the device when the incident light is *s*-polarized or *p*-polarized have been derived in our previous work.[28] They are defined and expressed in Eqs (1)–(4). The reflection coefficients corresponding to a s-incident light are

$$r_s = \frac{E_{rs}}{E_{is}} = \frac{2n_1\cos^2\alpha_i \cos\alpha_t \sin^2\theta}{n_1 \cos\alpha_t \left(\cos^2\theta + \cos^2\alpha_i \sin^2\theta\right) + n_2 \cos\alpha_i \cos\theta + n_2 \cos\alpha_i \cos^2\alpha_t \sin\theta} - 1, \tag{1}$$

$$r_p = \frac{E_{rp}}{E_{is}} = -\frac{2n_1 \cos\alpha_i \cos\alpha_t \sin\theta \cos\theta}{n_1 \cos\alpha_t \left(\cos^2\theta + \cos^2\alpha_i \sin^2\theta\right) + n_2 \cos\alpha_i \cos\theta + n_2 \cos\alpha_i \cos^2\alpha_t \sin\theta}. \tag{2}$$

When the incident light is p-polarized, the reflection coefficients become

$$r_s = \frac{E_{rs}}{E_{ip}} = \frac{2n_1 \cos\alpha_i \cos\alpha_t \sin\theta \cos\theta}{n_1 \cos\alpha_t \left(\cos^2\theta + \cos^2\alpha_i \sin^2\theta\right) + n_2 \cos\alpha_i \cos\theta + n_2 \cos\alpha_i \cos^2\alpha_t \sin\theta}, \tag{3}$$

$$r_p = \frac{E_{rp}}{E_{ip}} = 1 - \frac{2n_1 \cos\alpha_t \cos^2\theta}{n_1 \cos\alpha_t \left(\cos^2\theta + \cos^2\alpha_i \sin^2\theta\right) + n_2 \cos\alpha_i \cos\theta + n_2 \cos\alpha_i \cos^2\alpha_t \sin\theta}. \tag{4}$$

When the subwavelength-thick VO_2 film is in the insulating phase, it can be assumed to be a transparent layer and the theoretical equations are still satisfied. When the VO_2 was switched to the metallic phase, although it cannot be treated as a perfect conductive layer due to its limited sheet conductivity, it is expected to significantly change the output polarization state from the TIR geometry.

The polarization states of the reflected beam as a function of θ when the VO_2 layer was in the insulating phase were experimentally measured in a 6% relative humidity environment to first verify the theoretical equations. A right-angled fused silica prism was used to couple the THz light into the Si substrate. When the incident angle of the THz beam into the prism was 45°, the incident angle refracted onto the Si-VO_2 interface [α_i as shown in Fig. 1(c)] was 24.5°. The incident light was set as *s*-polarized and the *p*- and *s*-components in the reflected light were measured with different θ values. The reflected p- and s-signals in the time-domain with the θ value increasing from 0° to 90° were plotted in Figs. 2(a) and 2(b). The magnitude ratio $|E_{rp}/E_{rs}|$ and phase difference $\phi_p - \phi_s$ between the reflected *p*- and *s*-components were calculated and compared with the theoretical results, as shown in Figs. 2(c) and 2(d).

Figures 2(a) and 2(b) show the p- and s-signals reflected from the Si-VO_2-grating interface in the time-domain. The reflected p-component increased when θ increased from 0° to 47.5° and then decreased when θ kept increasing to 90°. The reflected s-component showed the opposite trend compared to the p-reflection and reached the minimum reflection at θ = 47.5°, as shown by the black curves in the figure. By applying a Fourier transform to the signals, we compared the magnitude

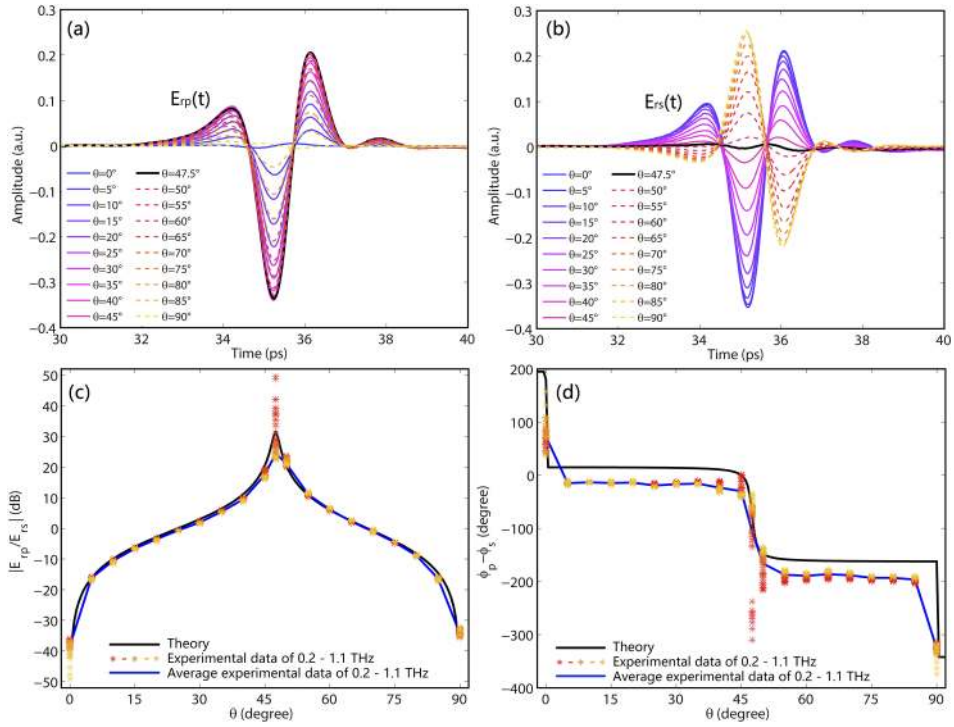

FIG. 2. Reflected (a) *p*- and (b) *s*-signals in the time-domain when θ increased from 0° to 90°. (c) Magnitude ratio $|E_{rp}/E_{rs}|$ in dB and (d) phase difference $\phi_p - \phi_s$ between the reflected *p*- and *s*-components. The star-dots from red to yellow show the experimental results from 0.2 THz to 1.1 THz. The blue curve shows the average result of the star-dots. The black curve shows the theoretical calculation result.

ratio and phase difference between the p- and s-reflections from 0.2 to 1.1 THz in Figs. 2(c) and 2(d). A nearly perfect match with the magnitude ratio is achieved. The matching of the star-dots with the theoretical lines indicates that the result is highly frequency-independent. The phase difference showed a very similar trend to the theory with an approximate 27° shift. Compared to the almost perfect phase matching in our previous work,[28] the small shift is expected to be caused by the thin film of VO_2 added as it shows a small conductivity in its insulating state. This can also be verified by comparing the phase difference between the reflected s-signals when θ = 0° and 90°, respectively. The s-reflection at θ = 0° is very close to the metal reflection with a 180° phase jump, while the s-reflection at θ = 90° is similar to the TIR from a Si-air interface when the VO_2 has zero conductivity. The theoretical phase difference of 115° can be calculated and is found to be different from the experimental phase difference of 145°, showing the effect of the non-zero conductivity of the VO_2. Both results in Figs. 2(c) and 2(d) show a larger deviation at θ = 0°, 47.5°, and 90° due to the nearly zero s- or p-reflections. From the comparison, we can conclude that the VO_2 layer has little effect on our theory. As shown in the example here, we can still predict the device output from our theoretical equations, and we can control it to function as an intensity modulator by rotating the grating with different θ values, or as a half-wave converter by setting θ to 47.5°.

A gate voltage was applied to the metallic grating to switch the underlying VO_2 film to the metallic state within the same measurement setup. The polarization state of the reflected THz light was measured to explore the polarization conversion of the VO_2 thin film in the metallic phase. The results of θ = 0°, 47.5°, and 90° are shown in Fig. 3. Figures 3(a) and 3(d) show the output polarization states when θ = 0° and when the VO_2 layer was in insulating and metallic phases, respectively. The results corroborated our expectation that the reflected signal maintains *s*-polarization when switching the VO_2 to the metallic phase. Because the grating was parallel to the polarization direction of the *s*-polarized input, the reflection from the grating was similar to the reflection off a metal surface when the VO_2 was in the insulating state and resulted in the s-polarized output. When the VO_2 was switched to the metallic phase, the reflection became a combination of the reflections from Si-VO_2 and

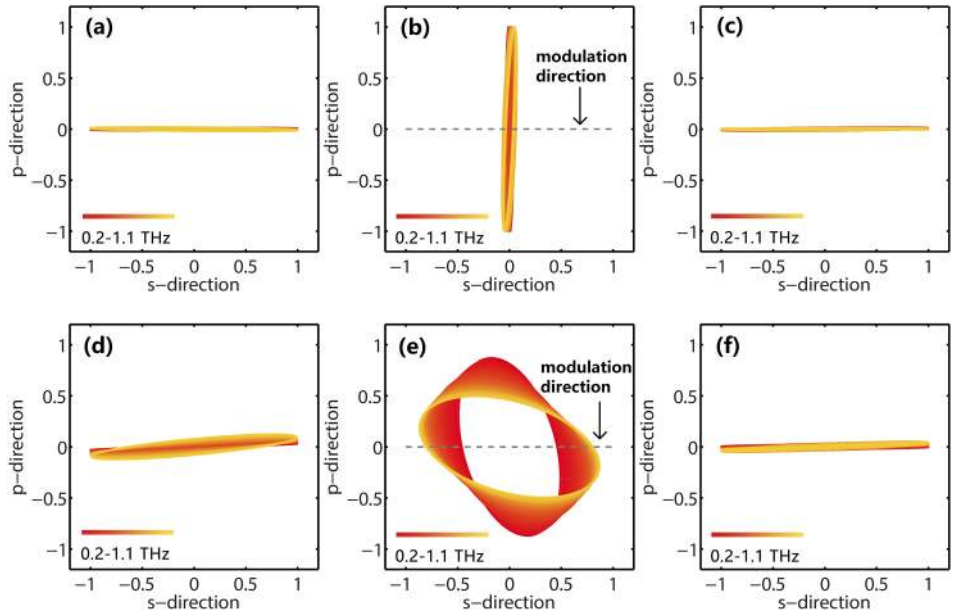

FIG. 3. The polarization states of reflected signals when the VO_2 was in the insulating state at (a) $\theta = 0°$, (b) $\theta = 47.5°$, and (c) $\theta = 90°$, and the polarization states of reflected signals when the VO_2 was in the metallic state at (d) $\theta = 0°$, (e) $\theta = 47.5°$, and (f) $\theta = 90°$. The dashed gray line in (b) and (e) indicates the intensity modulation in *s*-polarization.

VO_2-grating interfaces. Both reflections were s-polarized, and thus the polarization state maintained unchanged. Figures 3(c) and 3(f) are the reflections at $\theta = 90°$ when the VO_2 was in insulating and metallic states, respectively. When the VO_2 was in the insulating phase, the reflection was similar to that from a TIR from the Si-air interface and resulted in an *s*-polarized output. When the VO_2 was in the metallic phase, the reflection became a combination of the reflection from the Si-VO_2 interface and the TIR reflection from the VO_2-air interface. Neither of the reflections contributed any *p*-reflection component, and therefore the output was still *s*-polarized. Figures 3(b) and 3(e) show the reflections when $\theta = 47.5°$, and the VO_2 layer was in insulating and metallic phases, respectively. An obvious polarization conversion was observed. When the VO_2 was in the insulating state, the device functioned as a half-wave converter by converting the s-input to p-output. When switching the VO_2 to the metallic state, a strong field growth was found in the s-direction indicated by the gray lines in the figure, realizing a high-contrast intensity modulation in this direction. Due to the limited conductivity of VO_2 compared to the perfect conductive assumption, the reflection was not purely *s*-polarized. At the same time, the frequency-dependent conductivity of VO_2, especially at the low frequency region,[21,30] induced divergence to the polarization state. However, thanks to the almost zero intensity at the s-direction when the VO_2 was at the insulating state, a high and spectrally flat modulation can still be achieved in the effective 0.2-1.1 THz region. We calculated the modulation depth (MD) by $MD = (1 - I_{ins}/I_{met}) \times 100\%$, where I_{ins} and I_{met} are the field intensity when the VO_2 was in insulating and metallic phases, respectively. The MD as a function of frequency was calculated and plotted in Fig. 4.

A broadband modulation with maximum MD over 99.99% and an average modulation depth of 99.75% was achieved. The spectrally flat result indicates that the MD is almost frequency independent. Compared to the published devices employing VO_2 for intensity modulation in transmission geometry, the modulation depth of our device is much higher than the results in Refs. 24 and 25, and comparable to the work in Refs. 22 and 23. The working bandwidth in this example was narrower than some of the publications, but it is mainly limited by the absorption of the fused-silica prism and the system bandwidth. As can be observed from Fig. 3(e), the VO_2 showed a higher conductivity at the higher frequency region that contributed more s-components, indicating that the actual bandwidth of the device can be further extended by using a less-absorptive prism and a broader bandwidth system.

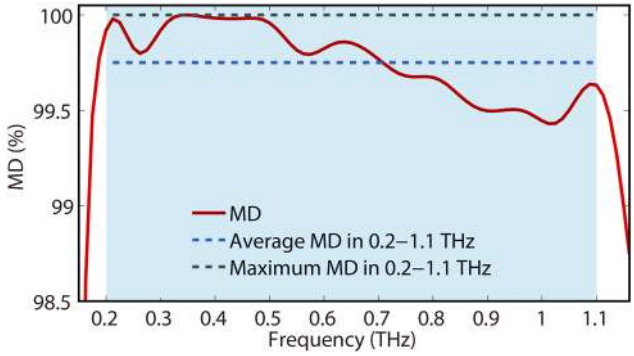

FIG. 4. The MD in the s-direction as a function of frequency.

To observe the polarization conversion ability of the device at higher frequencies, we replaced the right-angled fused-silica prism by a right-angled Si prism. The Si prism provided a much smaller absorption and extended the efficient working bandwidth up to 2 THz with the same THz system. In this case, a 45° incident angle was induced to the Si-VO_2 interface. When the incident signal was 45° linear polarized, the device worked as a 45° linear rotator, rotating the incident polarization direction for 45° to *p*-polarization at $\theta = 30°$. Therefore, the incident light was set to be 45° linear-polarized to measure the polarization state conversion of the reflected signal by the phase transition of VO_2. Figure 5(a) shows the output polarization state when the VO_2 was in the insulating phase. An almost linear *p*-polarized output was achieved, showing that our device can work as a 45° linear rotator. By applying a voltage to switch the VO_2 to the metallic phase, a circular polarized output from 0.8 to 1.5 THz was achieved, as shown in Fig. 5(b). The device worked as an active quarter-wave converter.

To better evaluate the polarization states, the (ε, ψ) system was used for description, as illustrated in Fig. 5(c). In Fig. 5(c), the ellipse represents the polarization state of the light, with a and b indicating the semi-major and semi-minor axes, respectively. ψ is the angle between a and the *s*-direction that represents the major polarization direction, whilst ε is calculated by $\varepsilon = \tan^{-1}(b/a)$ which represents

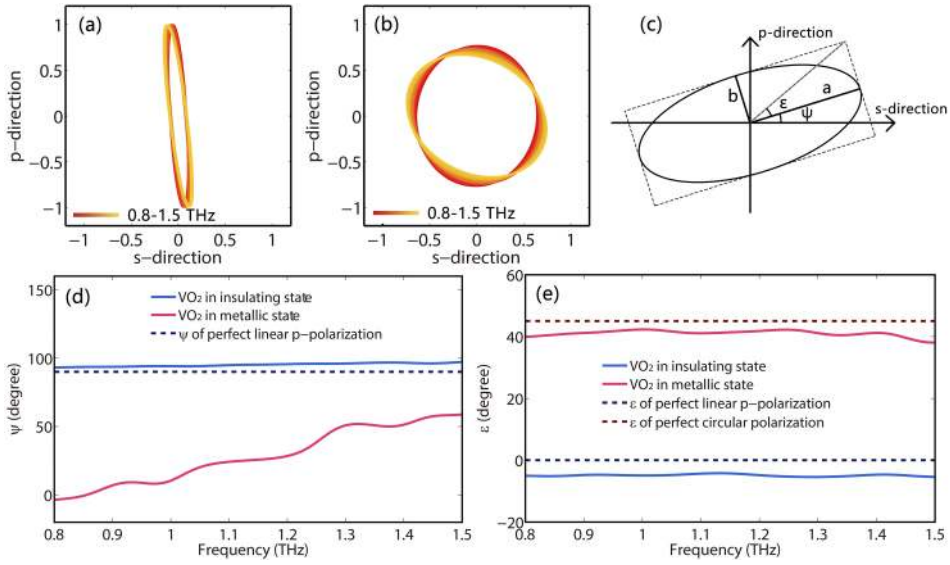

FIG. 5. The polarization states of reflected signals from 0.8 to 1.5 THz, when the VO_2 was in (a) insulating and (b) metallic states, respectively. (c) Schematic diagram of the (ε, ψ) system for describing the polarization state. (d) ψ and (e) ε of the reflected signal from 0.8 to 1.5 THz when the VO_2 was in insulating and metallic states are shown in solid curves, and the corresponding values of perfect linear p-polarization and perfect circular polarization are shown in dashed lines.

the ellipticity. ε has a minimum value of 0° representing a perfect linear polarization and a maximum value of 45° representing a perfect circular polarization state. The corresponding ε and ψ of the reflected signals when the VO_2 is in insulating and metallic phases are shown in Figs. 5(d) and 5(e). The dashed lines in Figs. 5(d) and 5(e) indicate the ideal values of perfect linear p-polarization and perfect circular polarization as a reference. When the VO_2 is in the insulating phase, the ψ value shows a deviation less than 8° to the ideal 90° in the 0.8-1.5 THz region, and the ε value is almost 0° with a deviation less than 6°. This indicates a very linear *p*-polarized output. The small component in the s-direction is most likely induced by the non-zero conductivity of the VO_2 layer in its insulating state. In this experiment, the s-reflection can be regarded as a combination of the s-reflections by the s-input component and the p-input component. Theoretically, these two reflections are fully out of phase, resulting in perfect destructive interference to give a zero output. However, as shown in the above verification experiment, the phase of the reflection coefficients slightly deviated from the theory. The combination of these two reflections is no longer perfectly destructively interfering, leaving a small signal in this direction. When switching VO_2 to the metallic state, the ε value was very close to the ideal 45° with a variation less than 7° in the studied range. The ψ value in this case has little meaning when ε is close to 45° as it only indicates the major orientation trend of the weak elliptical shape. The results show a nearly perfect circular-polarization output with a few oscillations and offset; these are most likely to be induced by slight non-uniformity of the grating structure due to the fabrication tolerance. The results demonstrated that an electrical switch between linear *p*-polarized and circular-polarized reflections in the ultra-broad 0.8-1.5 THz region was achieved. The device behaves as an active broadband quarter-wave converter. In previous reports on active THz quarter-waveplates, Hsieh *et al.* realized similar conversion by using liquid crystal birefringence, but this could only be performed in a very narrow bandwidth,[31] as the propagation-induced phase change is frequency dependent. Wang *et al.* also utilized the phase transition property of VO_2 to make a switchable quarter-waveplate.[32] However, their device only shifted the quarter-wave working frequency for 34 GHz rather than switching it on and off, and the combination with a metamaterial structure made it a single frequency device. Our approach represents the first demonstration of an ultra-broad bandwidth actively switched quarter-wave conversion.

Only two experimental examples with the above two sets of incident angles are reported in this article. There are actually many more potential experiments with different combinations of incident angle, θ value, and incident polarization state to be researched. Our proof-of-principle design opens the way for electrically controlling the polarization state of THz light on a broad band, using a relatively simple approach. Different incident angles, θ values, incident polarization states, or even different substrates can be carefully selected according to specific working bandwidths or different purposes of the polarization control.

The modulation speed of the device is in the region of a few tens of seconds, which is limited by the VO_2 phase transition properties. The detailed reasons for the delay-time of turning on and off the VO_2 device and approaches to improve the modulation speed have been explained by Han *et al.*[33] As the turning on time is positively related to the VO_2 thickness and area, one method is to restrain the VO_2 area in the regions in between the grating wires to shorten the onset of the phase transition and improving the on-state switch speed.

CONCLUSIONS

In this work, a flexible and multifunctional design for polarization control of THz waves was demonstrated. The device is built as a 100 nm thick VO_2 layer on a Si substrate combined with a metal grating structure on top of the VO_2 layer. The grating also operates as electrodes to electrically activate the VO_2 phase transition. The sample was attached to a suitable prism to realize TIR at the Si-grating interface. When the VO_2 layer was in the insulating phase, the device followed the expected theoretical behavior and operated as a multifunctional polarization converter that can realize quarter-wave and half-wave conversions or other linear rotations. When switching the VO_2 into the metallic phase, the polarization state of the reflected signal can be electrically controlled with a proper parameter combination of α_i, θ, and the incident polarization state. In the setup of $\alpha_i = 24.5°$, $\theta = 47.5°$, and *s*-polarized incident light, the device demonstrated an averaged broadband intensity modulation

of 99.75% in the frequency range of 0.2-1.1 THz. The bandwidth could be further extended by using a low-loss prism. Whilst in the setup of $\alpha_i = 45°$, $\theta = 30°$, and 45°-polarized incident light, the device became an ultra-broadband active quarter-wave converter that can be switched between a linear p-polarization state and a circular polarization state for 0.8-1.5 THz. This TIR design, which can be easily integrated with typical THz systems, opens the way for actively controlling polarization states of the THz light in an ultra-broad bandwidth.

ACKNOWLEDGMENTS

Partial financial support for this work was received from the Hong Kong Research Grants Council (Project Nos. 14201415 and 14205514) and the Hong Kong Innovation Technology Fund (Project No. ITS/291/14).

[1] E. P. J. Parrott and J. A. Zeitler, Appl. Spectrosc. **69**, 1 (2015).
[2] P. U. Jepsen, D. G. Cooke, and M. Koch, Laser Photonics Rev. **5**, 124 (2011).
[3] Q. Sun, Y. He, K. Liu, S. Fan, E. P. J. Parrott, and E. Pickwell-MacPherson, Quant. Imaging Med. Surg. **7**, 345 (2017).
[4] R. K. May, M. J. Evans, S. Zhong, I. Warr, L. F. Gladden, Y. Shen, and J. A. Zeitler, J. Pharm. Sci. **100**, 1535 (2011).
[5] J. A. Zeitler and L. F. Gladden, Eur. J. Pharm. Biopharm. **71**, 2 (2009).
[6] B. Clough, J. Dai, and X.-C. Zhang, Mater. Today **15**, 50 (2012).
[7] X.-C. Zhang and J. Xu, *Introduction to THz Wave Photonics* (Springer, New York, 2010).
[8] A. Partanen, J. Väyrynen, S. Hassinen, H. Tuovinen, J. Mutanen, T. Itkonen, P. Silfsten, P. Pääkkönen, M. Kuittinen, K. Mönkkönen, and T. Venäläinen, Appl. Opt. **51**, 8360 (2012).
[9] Z. Huang, H. Park, E. P. J. Parrott, H. P. Chan, and E. Pickwell-MacPherson, IEEE Photonics Technol. Lett. **25**, 81 (2013).
[10] Z. Huang, E. P. J. Parrott, H. Park, H. P. Chan, and E. Pickwell-MacPherson, Opt. Lett. **39**, 793 (2014).
[11] L. Y. Deng, J. H. Teng, L. Zhang, Q. Y. Wu, H. Liu, X. H. Zhang, and S. J. Chua, Appl. Phys. Lett. **101**, 11101 (2012).
[12] I. Yamada, K. Takano, M. Hangyo, M. Saito, and W. Watanabe, Opt. Lett. **34**, 274 (2009).
[13] L. Ren, C. L. Pint, T. Arikawa, K. Takeya, I. Kawayama, M. Tonouchi, R. H. Hauge, and J. Kono, Nano Lett. **12**, 787 (2012).
[14] B. Lu, H. Wang, J. Shen, J. Yang, H. Mao, L. Xia, W. Zhang, G. Wang, X.-Y. Peng, and D. Wang, AIP Adv. **6**, 25215 (2016).
[15] L. Cong, W. Cao, X. Zhang, Z. Tian, J. Gu, R. Singh, J. Han, and W. Zhang, Appl. Phys. Lett. **103**, 171107 (2013).
[16] H. Chen, W. J. Padilla, M. J. Cich, A. K. Azad, R. D. Averitt, and A. J. Taylor, Nat. Photonics **3**, 148 (2009).
[17] C. Han, E. P. J. Parrott, and E. Pickwell-Macpherson, IEEE J. Sel. Top. Quantum Electron. **23**, 4700806 (2017).
[18] L. Cong, N. Xu, J. Gu, R. Singh, J. Han, and W. Zhang, Laser Photonics Rev. **8**, 626 (2014).
[19] M. Scheller, C. Jördens, and M. Koch, Opt. Express **18**, 10137 (2010).
[20] B. Scherger, M. Scheller, N. Vieweg, S. T. Cundiff, and M. Koch, Opt. Express **19**, 24884 (2011).
[21] P. U. Jepsen, B. M. Fischer, A. Thoman, H. Helm, J. Y. Suh, R. Lopez, and R. F. Haglund, Phys. Rev. B **74**, 205103 (2006).
[22] M. Seo, J. Kyoung, H. Park, S. Koo, H. Kim, H. Bernien, B. J. Kim, J. H. Choe, Y. H. Ahn, H.-T. Kim, N. Park, Q.-H. Park, K. Ahn, and D. Kim, Nano Lett. **10**, 2064 (2010).
[23] Y.-G. Jeong, H. Bernien, J.-S. Kyoung, H.-R. Park, H.-S. Kim, J.-W. Choi, B.-J. Kim, H.-T. Kim, K. J. Ahn, and D.-S. Kim, Opt. Express **19**, 21211 (2011).
[24] E. P. J. Parrott, C. Han, F. Yan, G. Humbert, A. Bessaudou, A. Crunteanu, and E. Pickwell-MacPherson, Nanotechnology **27**, 205206 (2016).
[25] J.-H. Shin, K. Moon, E. S. Lee, I.-M. Lee, and K. Hyun Park, Nanotechnology **26**, 315203 (2015).
[26] X. Liu, Z. Chen, E. P. J. Parrott, B. S.-Y. Ung, J. Xu, and E. Pickwell-MacPherson, Adv. Opt. Mater. **5**, 1600697 (2017).
[27] X. Liu, E. P. J. Parrott, B. S.-Y. Ung, and E. Pickwell-MacPherson, APL Photonics **1**, 76103 (2016).
[28] X. Liu, X. Chen, E. P. J. Parrott, and E. Pickwell-MacPherson, Photonics Res. **5**, 299 (2017).
[29] V. Théry, A. Boulle, A. Crunteanu, J. C. Orlianges, A. Beaumont, R. Mayet, A. Mennai, F. Cosset, A. Bessaudou, and M. Fabert, J. Appl. Phys. **121**, 55303 (2017).
[30] T. L. Cocker, L.V. Titova, S. Fourmaux, D. Brassard, M. A. El Khakani, and F. A. Hegmann, Appl. Phys. Lett. **97**, 221905 (2010).
[31] C.-F. Hsieh, R.-P. Pan, T.-T. Tang, H.-L. Chen, and C.-L. Pan, Opt. Lett. **31**, 1112 (2006).
[32] D. Wang, L. Zhang, Y. Gu, M. Q. Mehmood, and Y. Gong, Sci. Rep. **5**(1), 15020 (2015).
[33] C. Han, E. P. J. Parrott, G. Humbert, A. Crunteanu, and E. Pickwell-macpherson, Sci. Rep. **7**, 12725 (2017).